Development of Rimless Wheel with Controlled Wobbling Mass

doi: https://doi.org/10.1109/IROS.2018.8593812

Development of Rimless Wheel with Controlled Wobbling Mass

Yuta Hanazawa

***Abstract*— This paper presents a novel method for generating level-ground walking for a rimless wheel with a controlled wobbling mass. Our rimless wheel achieves level-ground walking by simply controlling the wobbling mass attached to the wheel. We mathematically demonstrate that the controlled wobbling mass generates propulsive effects for the rimless wheel. The walking speed of the rimless wheel can be changed by varying the amplitude of the wobbling mass: thus slow walking to high-speed walking can be realized for the wheel. Moreover, we have developed a robot based on a rimless wheel to show effectiveness of our proposed methods. We then analyze the walking properties with respect to the physical parameters and control parameters of our robot through numerical simulation.**

I. INTRODUCTION

In dynamic walking research, wheels without rims are known as rimless wheels. A rimless wheel is one of the simplest biped walking model. Researchers have explored method to generate biped walking motion. McGeer demonstrated passive dynamic walking on a slope and the analogy between the passive dynamic walking of a biped robot and the rotation of a rimless wheel [1]. Passive dynamic walking is an efficient walking pattern generation method, and many walking pattern generation methods based on passive dynamic walking have been developed [2]–[9].

Recently, the use of contolled rimless wheels as mobile robot is being studied. Kawamoto et al. and Asano et al. demonstrated level-ground walking that is achieved using a rimless wheel with a torso with viscoelastic legs [10], [11]. The rimless wheel can achieve level-ground walking via manipulation of the torso posture and can overcome irregular terrains. Moreover, it may be possible to develop mobile robots based on rimless wheels with excellent mobility.

To realize the propulsive effect of the rimless wheel on level ground, the rimless wheel must tilt or rotate the torso while walking. However, we do not want the torso to be tilted when the rimless wheel transports cargo or humans. Therefore, if we can generate propulsive effects in rimless wheels without tilting the torso, a novel rimless wheel that can walk on level-ground with variable speed can be developed.

For this purpose, we utilize an actively controlled wobbling mass. We proposed a walking pattern generation method for biped robots via active control of the wobbling mass [12]. The actively controlled wobbling mass generate

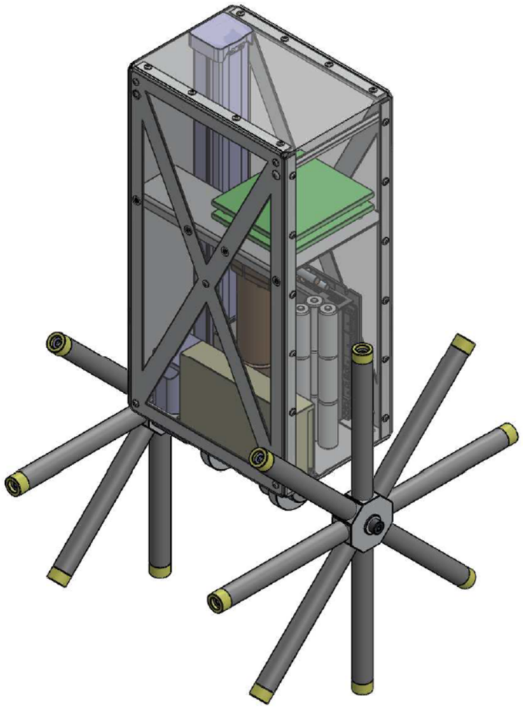

Fig. 1. 3D-CAD model of RW-3

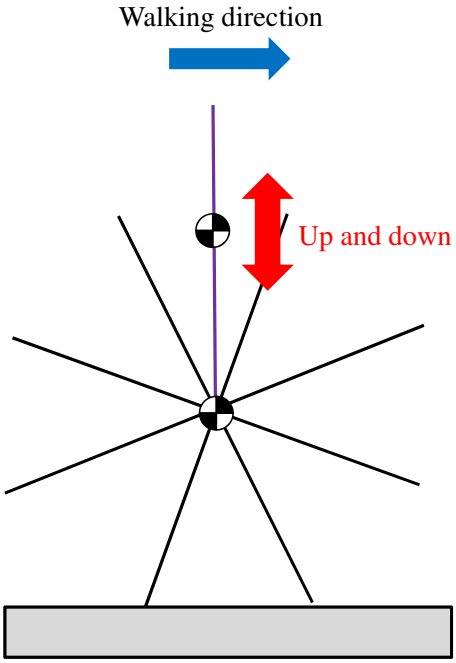

Fig. 2. Schematic of the proposed rimless wheel with the torso

[1]Y. Hanazawa is with the Dept. of Applied Science for Integrated System Engineering, Graduate School of Engineering, Kyushu Institute of Technology, 1-1 Sensui, Tobata, Kitakyushu, Fukuoka 804-8550, JAPAN hanazawa-y@ise.kyutech.ac.jp

a propulsive effect for the biped robot, thus realizing high-speed level-ground walking. We apply rimless wheels to generate this propulsive effect by using the controlled wobbling mass. We expect that our rimless wheel can achieve various walking speed without tilting the torso by our proposed method. Moreover, we have developed a novel robot based on the rimless wheel. The robot name is RW-3(Rimless Wheel Walker with Wobbling mass) as shown in Fig. 1.

In this paper, we demonstrate a novel propulsive effects generation method for the rimless wheel using a controlled wobbling mass as shown in Fig. 2. Moreover, since we do not complete construction of RW-3 yet, we show outline of RW-3 using 3D-CAD model. We mathematically establish the propulsive effect generated by the controlled wobbling mass and prove the effectiveness of the proposed method via the numerical simulation.

II. MODEL OF RW-3

A. Dynamic Equation

The proposed model is schematized in Fig. 3. RW-3 has a torso with a wobbling mass. The wobbling mass can move up and down because of a linear actuator. The dynamic equation of RW-3 is given by

$$\boldsymbol{M}(\boldsymbol{q})\ddot{\boldsymbol{q}} + \boldsymbol{H}(\boldsymbol{q}, \dot{\boldsymbol{q}}) = \boldsymbol{S}\boldsymbol{u} + \boldsymbol{J}_c^{\mathrm{T}}\boldsymbol{\lambda}, \tag{1}$$

where $\boldsymbol{q} = [\theta_1,\ \theta_2,\ l_b,\ x_1,\ z_1]^{\mathrm{T}}$is the generalized coordinate vector, $\boldsymbol{M}(\boldsymbol{q}) \in \mathbb{R}^{5\times5}$ is the inertia matrix, $\boldsymbol{H}(\boldsymbol{q}, \dot{\boldsymbol{q}}) \in \mathbb{R}^5$ is a vector comprising the Coriolis force, centrifugal force, and gravitational vector, and $\boldsymbol{u} = [u_1,\ u_2]^{\mathrm{T}}$ is the input vector, $\boldsymbol{S} \in \mathbb{R}^{5\times2}$ is the following driving matrix:

$$\boldsymbol{S} = \begin{bmatrix} -1 & 0 \\ 1 & 0 \\ 0 & 1 \\ 0 & 0 \\ 0 & 0 \end{bmatrix}.$$

$\boldsymbol{J}_c \in \mathbb{R}^{N\times5}$ is the Jacobian matrix, which is determined under N constraint conditions of the robot. The constraint force vector $\boldsymbol{\lambda} \in \mathbb{R}^N$ is given by

$$\boldsymbol{\lambda} = -\boldsymbol{X}(\boldsymbol{q})^{-1}(\boldsymbol{J}_c\boldsymbol{M}_B(\boldsymbol{q})^{-1}\boldsymbol{\Gamma}(\boldsymbol{q},\dot{\boldsymbol{q}},\boldsymbol{u}) + \dot{\boldsymbol{J}}_c\dot{\boldsymbol{q}}), \tag{2}$$

where

$$\boldsymbol{X}(\boldsymbol{q}) = \boldsymbol{J}_c\boldsymbol{M}_B(\boldsymbol{q})^{-1}\boldsymbol{J}_c^{\mathrm{T}}, \tag{3}$$

$$\boldsymbol{\Gamma}(\boldsymbol{q}, \dot{\boldsymbol{q}}, \boldsymbol{u}) = \boldsymbol{S}\boldsymbol{u} - \boldsymbol{H}(\boldsymbol{q}, \dot{\boldsymbol{q}}). \tag{4}$$

B. Constraint Conditions of the Robot

The leg tip of the rimless wheel is in contact with the ground. Thus, it is constrained on the ground, and the constraint equations are given as follows:

$$\dot{x}_1 = 0, \tag{5}$$

$$\dot{z}_1 = 0. \tag{6}$$

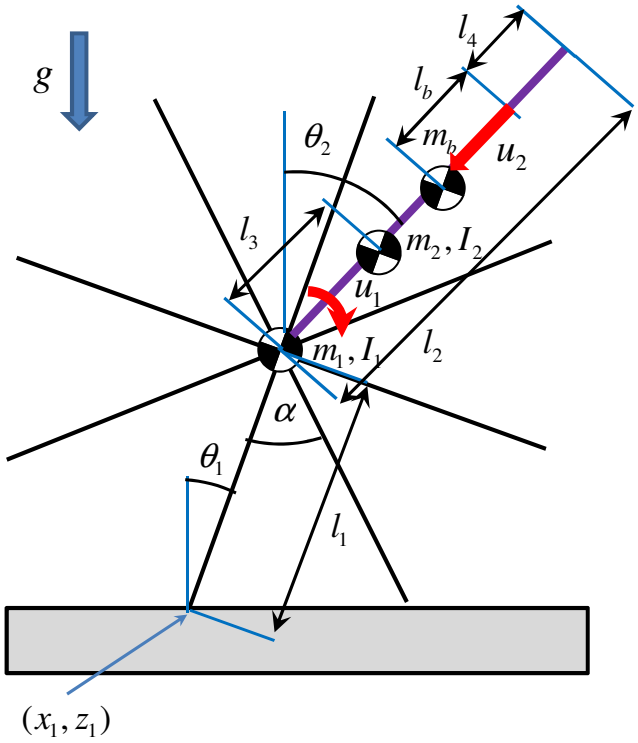

Fig. 3. Model of RW-3

From these equations, $\boldsymbol{J}_c \in \mathbb{R}^{2\times5}$ and $\dot{\boldsymbol{J}}_{\boldsymbol{c}} \in \mathbb{R}^{2\times5}$ are obtained as

$$\boldsymbol{J}_c\dot{\boldsymbol{q}} = \begin{bmatrix} 0 & 0 & 0 & 1 & 0 \\ 0 & 0 & 0 & 0 & 1 \end{bmatrix}\dot{\boldsymbol{q}} = \boldsymbol{0}_{2\times1}, \tag{7}$$

$$\dot{\boldsymbol{J}}_c = \boldsymbol{0}_{2\times5}. \tag{8}$$

C. Impact Equation

The collision of the leg with the ground is assumed to be inelastic and instantaneous. The velocity of the robot immediately after a collision is obtained from the impact equation [13]. When the leg tip touches the ground, the constraint equation $\boldsymbol{J}_I \in \mathbb{R}^{2\times5}$ of the robot is given by

$$\boldsymbol{J}_I\dot{\boldsymbol{q}} = \begin{bmatrix} l_1\cos\theta_1 - l_1\cos(\alpha-\theta_1) & 0 & 0 & 1 & 0 \\ -l_1\sin\theta_1 - l_1\sin(\alpha-\theta_1) & 0 & 0 & 0 & 1 \end{bmatrix}\dot{\boldsymbol{q}} = \boldsymbol{0}_{2\times1}. \tag{9}$$

The impulse vector, $\boldsymbol{\lambda}_I \in \mathbb{R}^2$ and the velocity vector immediately after impact, $\dot{\boldsymbol{q}}^+ \in \mathbb{R}^5$ are respectively given by

$$\boldsymbol{\lambda}_I = -\boldsymbol{X}_I(\boldsymbol{q})^{-1}\boldsymbol{J}_I\dot{\boldsymbol{q}}^-, \tag{10}$$

$$\dot{\boldsymbol{q}}^+ = (\boldsymbol{I}_{5\times5} - \boldsymbol{M}(\boldsymbol{q})^{-1}\boldsymbol{J}_I^{\mathrm{T}}\boldsymbol{X}_I(\boldsymbol{q})^{-1}\boldsymbol{J}_I)\dot{\boldsymbol{q}}^-, \tag{11}$$

where $\boldsymbol{X}_I(\boldsymbol{q}) := \boldsymbol{J}_I\boldsymbol{M}(\boldsymbol{q})^{-1}\boldsymbol{J}_I^{\mathrm{T}}$ and $\dot{\boldsymbol{q}}^- \in \mathbb{R}^5$ is the velocity immediately before impact.

III. EFFECT OF THE WOBBLING MASS

In this section, we explain the propulsive effects due to the wobbling mass.

Fig. 4 and Fig. 5 show schematic of the rimless wheel when the wobbling mass goes down in the negative stance

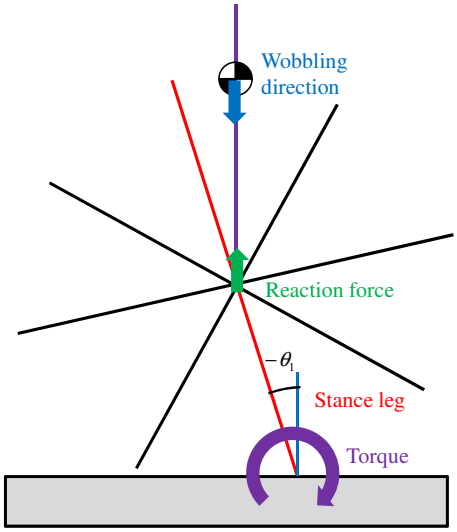

Fig. 4. Schematic of the rimless wheel with the wobbling mass going up in the negative stance leg angle

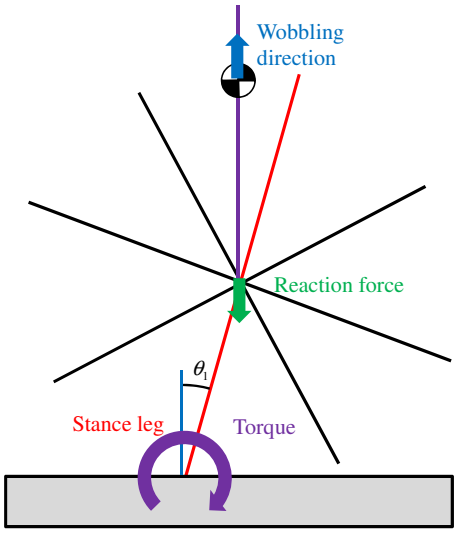

Fig. 5. Schematic of rimless wheel with the wobbling mass going down in the positive stance leg angle

leg angle and when it goes up in the positive stance leg angle. In both cases torque is generated by the reaction force due to the wobbling of the mass, and this torque generates the propulsive effects.

We designed the desired trajectory of the wobbling mass for generating the propulsive effect. Fig. 6 shows a schematic of the desired wobbling mass trajectory and the hip mass of the rimless wheel trajectory. The desired wobbling mass trajectory is antiphase with respect to the hip mass of the rimless wheel trajectory. Therefore, we synchronize the desired wobbling mass trajectory with the hip mass trajectory.

IV. CONTROL METHODS

The input for torso control is given by

$$u_1 = -K_{P1}(\theta_2 - \theta_{2d}) - K_{D1}\dot{\theta}_2, \tag{12}$$

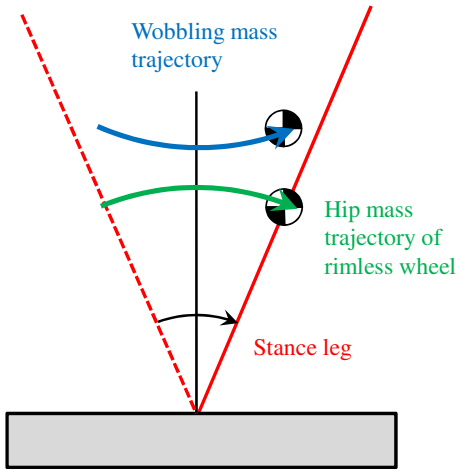

Fig. 6. Schematic of the wobbling mass and hip mass trajectories for generating propulsive effects

where K_{P1} and K_{D1} are the control gains, and θ_{2d} is the desired torso angle. This input achieves the static torso angle. The input for the wobbling mass is then given by

$$u_2 = -K_{P2}(l_b - l_{bd}) - K_{D2}(\dot{l}_b - \dot{l}_{bd}), \tag{13}$$

where K_{P2} and K_{D2} are the control gains. Moreover, l_{bd} is the desired wobbling mass position, which is expressed as follows:

$$l_{bd} = -K_a(P_z - d_1) + d_2. \tag{14}$$

where K_a is the amplitude of wobbling, P_z is the height of the center of the rimless wheel d_1 and d_2 are the control parameters of the motion of the wobbling mass. Furthermore, $\dot{l}_{bd}$ is the desired wobbling mass velocity and is expressed as follows:,

$$\dot{l}_{bd} = K_a(\dot{z}_1 - l_1 \sin\theta_1 \dot{\theta}_1). \tag{15}$$

This input achieves that the wobbling mass trajectory is antiphase with respect to the hip mass trajectory. Thus, the rimless wheel generates propulsive effects and realizes level-ground walking. Moreover, we can freely change the propulsive effects by the amplitude of the wobbling mass, K_a. The rimless wheels can realize a wide range walking speed.

V. DESIGN OF RW-3

We have designed RW-3 as shown Fig. 1. Figs. 7, 8 and 9 show front view, side view and top view of the robot, respectively. The frame of RW-3 is aluminum to achieve a tough and light weight robot. We can observe the motion of the wobbling mass since the body is made of clear polycarbonate plates. The height of the robot is about 0.67 m and the weight of the robot is about 12 kg. The actuator for the wobbling mass is MISUMI linear actuator RS112-R-P1-1-300. Moreover, we selected an actuator for the torso that is Maxon motor EC45-250 W. We consider that the robot is controlled by remote control using a joystick.

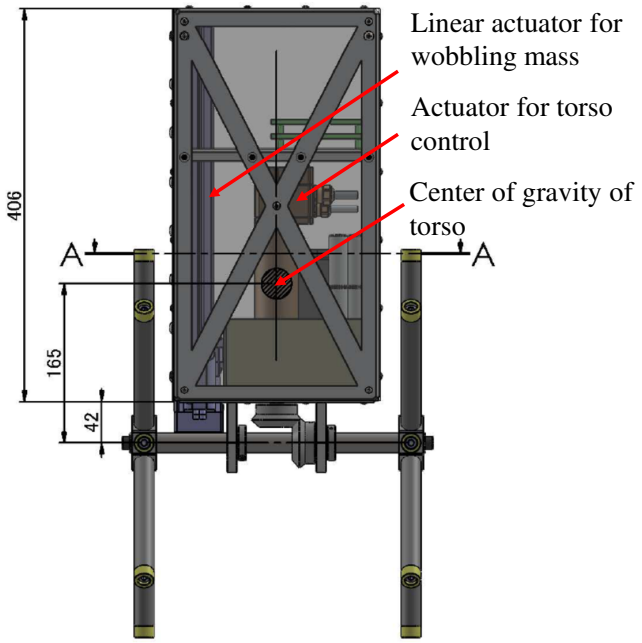

Fig. 7. Front view of RW-3

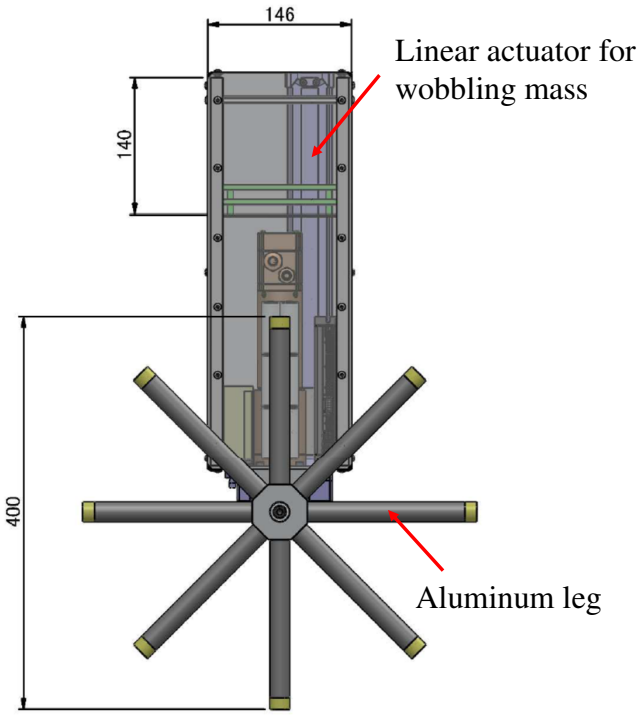

Fig. 8. Side view of RW-3

VI. Walking Analysis

In this section, we present the analysis of the walking performance of RW-3 through numerical simulation.

A. Achievement of periodic walking

We set the physical parameters of RW-3 as presented in Table I and the control parameters as presented in Table II. We set the initial parameter as follows: $\boldsymbol{q} = [0.0,\ 0.0,\ 0.0,\ 0.0,\ 0.0]^{\mathrm{T}}$ and $\dot{\boldsymbol{q}} = [2.0,\ 0.0,\ 0.0,\ 0.0,\ 0.0]^{\mathrm{T}}$ Moreover, the torque limit and force limit were set as 50 Nm and 50 N, respectively. The average walking speed is 0.43 m/s and the specific resistance (SR) is 0.50 for 10 steps. SR is the index of the energy efficiency of dynamic walking is given as follows: The SR is given by

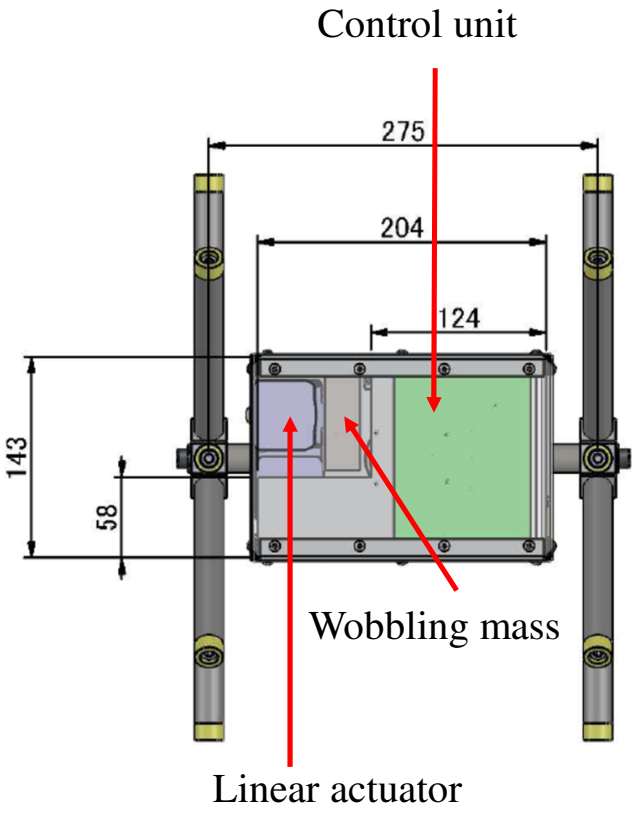

Fig. 9. Top view of RW-3

$$\mathrm{SR} := \frac{p}{Mgv}, \tag{16}$$

where p [J/s] is the average input power, M [kg] is the total mass of the robot, and v [m/s] is the average walking speed. The average input power, p, is given by

$$p := \frac{1}{T}\int_0^T (|u_1(\dot{\theta}_2 - \dot{\theta}_1)| + |u_2 \dot{l}_b|)\mathrm{d}t,$$

where T [s] is the total walking time.

Fig. 10 shows the stick diagram of the level-ground walking for 10 steps. RW-3 walked on level ground without stopping. Then, we confirmed the wobbling mass trajectory and hip mass trajectory. Fig. 11 shows the wobbling mass trajectory (magenta) and hip mass trajectory (green). We can see that the wobbling mass trajectory is antiphase with respect to the hip mass trajectory. Our control method achieves the desired wobbling mass trajectory, and the motion of the wobbling mass generates propulsive effects.

Fig. 12 and Fig. 13 show the force for the wobbling mass and torque for the torso with respect to time, respectively. The force and torque vary periodically during the walking motion. Fig. 14 shows the total mechanical energy during

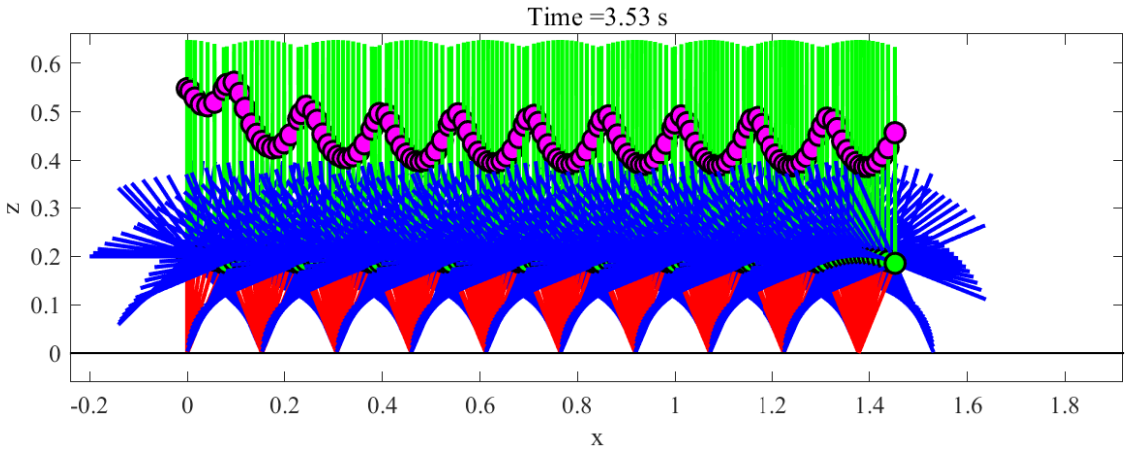

Fig. 10. Stick diagram of level-ground walking

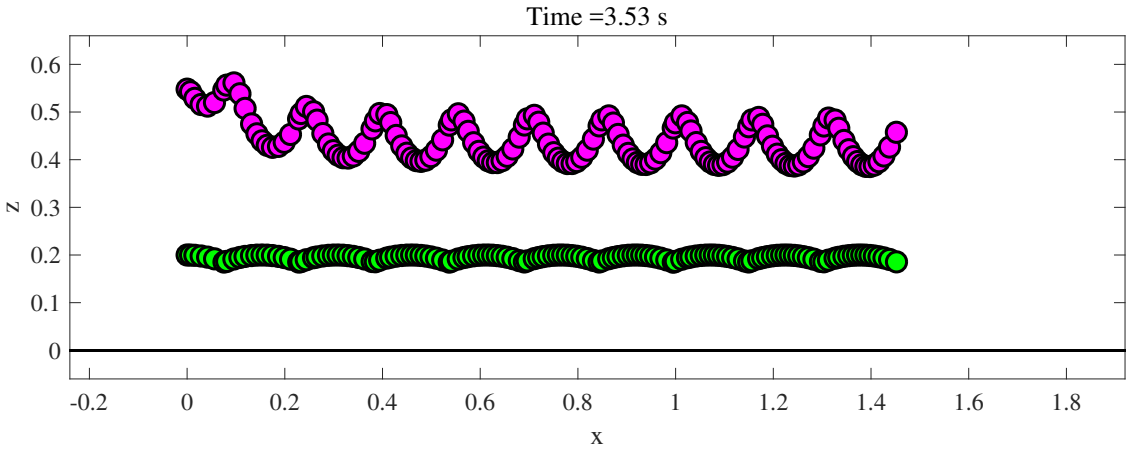

Fig. 11. Wobbling mass trajectory (magenta) and hip mass trajectory (green)

TABLE I
PHYSICAL PARAMETERS IN THE SIMULATIONS

Symbol	Value	Unit
m_1	3.36	kg
m_2	7.80	kg
m_b	2.0	kg
l_1	0.2	m
l_2	0.448	m
l_3	0.165	m
l_4	0.1	m
I_1	0.0323	kg $\cdot$ m^2
I_2	0.1092	kg $\cdot$ m^2
g	9.8	m/s^2
α	$\pi/4$	rad

TABLE II
CONTROL PARAMETERS IN THE SIMULATIONS

Symbol	Value	Unit
K_{P1}	2000	Nm/rad
K_{D1}	200	Nm/(rad/s)
θ_{2d}	0.0	rad
K_{P2}	2000	N/m
K_{D2}	500	N/(m/s)
d_1	0.2	m
d_2	0.203	m
K_a	8.0	-

the walking motion with respect to time. The variation in mechanical energy is periodic, and it converges to approximately 43-46 J. From these results, we see that upon applying our method, the walking of RW-3 converges to 1-periodic limit cycle walking.

B. Walking variation via mass and amplitude of the wobbling mass

Figs. 15 and 16 show the average walking speed for 10 step and SR, respectively, with respect to mass of wobbling mass. We see that the walking speed increases monotonically when the mass of wobbling mass is large. The SR increases monotonically when the mass of wobbling mass is large.

Figs. 17 and 18 show the average walking speed for 10 step and SR, respectively, with respect to the amplitude of

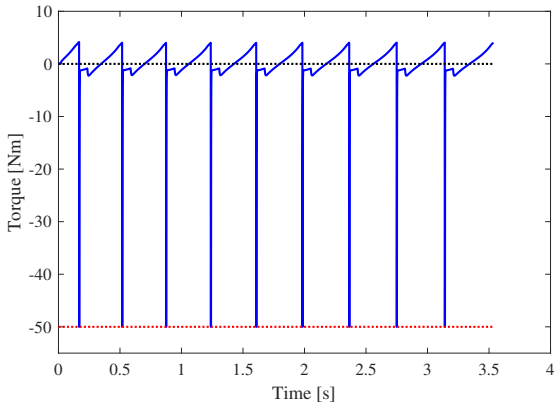

Fig. 12. Torque for maintaining torso with respect to time

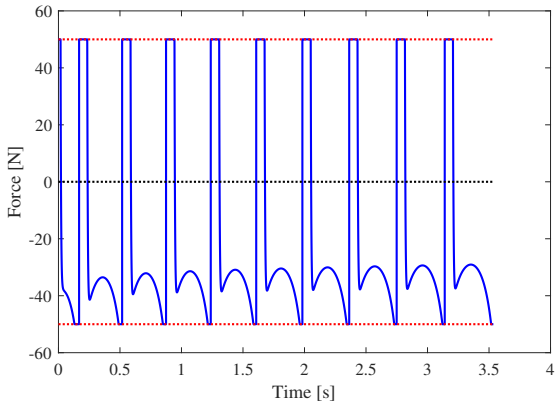

Fig. 13. Force for going up and down wobbling mass with respect to time

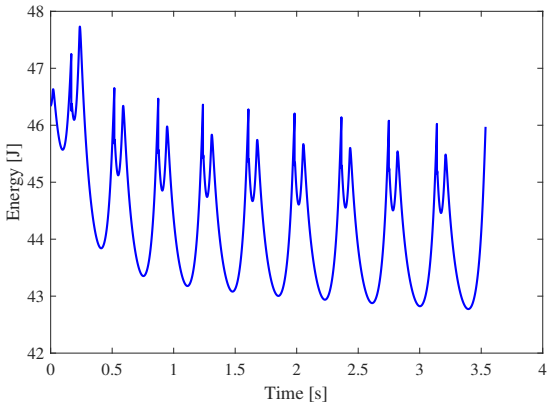

Fig. 14. Mechanical energy during the walking motion with respect to time

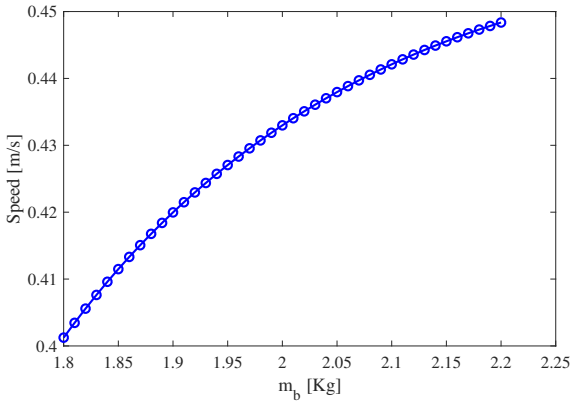

Fig. 15. Walking speed of RW-3 with respect to the mass of the wobbling mass

the wobbling mass. When the amplitude of wobbling mass is large, that the walking speed increases monotonically, and SR increases monotonically.

The effect of the wobbling mass is large when the mass and amplitude of wobbling mass are large. Thus, we can set the speed of RW-3 by the choosing the mass and amplitude of wobbling mass.

VII. CONCLUSION

In this study, we developed a novel rimless wheel with an actively controlled wobbling mass. We first showed the design of RW-3 as a robot achieving level ground walking. RW-3 can walk on level-ground without tilting or rotating its torso. We can freely change the walking speed by controlling to the mass and amplitude of the wobbling mass. Thus, the rimless wheel can realize a wide range of walking speeds.

Fig. 19 shows the prototype of RW-3. We have finished the design of RW-3, and started assemblage of RW-3. We further aim to conduct walking experiments on irregular terrains. Moreover, we must compare our rimless wheel with other mobile robots in terms of efficiency, speed, and robustness.

ACKNOWLEDGMENT

The author wish to thank ONO-DENKI CO., LTD. for many helpful technical supprts for RW-3. This research was partially supported by JSPS KAKENHI Grant-in-Aid for Young Scientists (B) with Grant Number 15K18090.

REFERENCES

[1] T. McGeer, "Passive dynamic walking," *The International Journal of Robotics Research*, vol. 9, no. 2, pp. 62–82, 1990.

[2] F. Asano, M. Yamakita, and K. Furuta, "Virtual passive dynamic walking and energy-based control laws," in *Proc. IEEE/RSJ International Conference on Intelligent Robots and Systems (IROS)*, 2002, pp. 1149–1154.

[3] M. Wisse, "Three additions to passive dynamic walking; actuation, an upper body, and 3D stability," in *Proc. IEEE/RAS International Conference on Humanoid Robots (HUMANOIDS)*, vol. 1, 2004, pp. 113–132.

[4] S. H. Collins, A. Ruina, R. Tedrake, and M. Wisse, "Efficient bipedal robots based on passive-dynamic walkers," *Science*, vol. 307, no. 5712, pp. 1082–1085, 2005.

[5] D. G. E. Hobbelen and M. Wisse, *"*Limit cycle walking*", Humanoid Robots, Human-like Machines,* chapter 14. InTech, 2007.

[6] D. Hobbelen, T. de Boer, and M. Wisse, "System overview of bipedal robots flame and tulip: Tailor-made for limit cycle walking," in *Proc. IEEE/RSJ International Conference on Intelligent Robots and Systems (IROS)*, 2008, pp. 2486–2491.

[7] K. Narioka, S. Tsugawa, and K. Hosoda, "3d limit cycle walking of musculoskeletal humanoid robot with flat feet," in *Proc. IEEE/RSJ International Conference on Intelligent Robots and Systems (IROS)*, 2009, pp. 4676–4681.

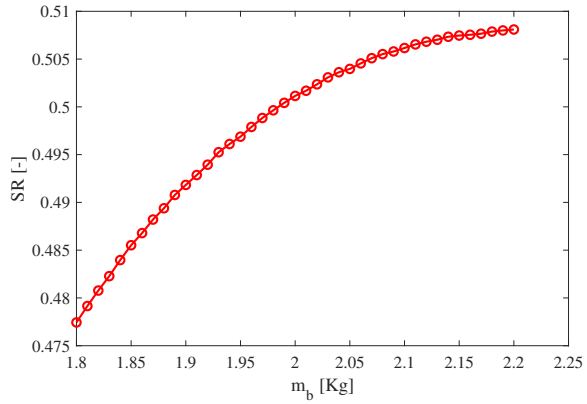

Fig. 16. SR of RW-3 with respect to the mass of the wobbling mass

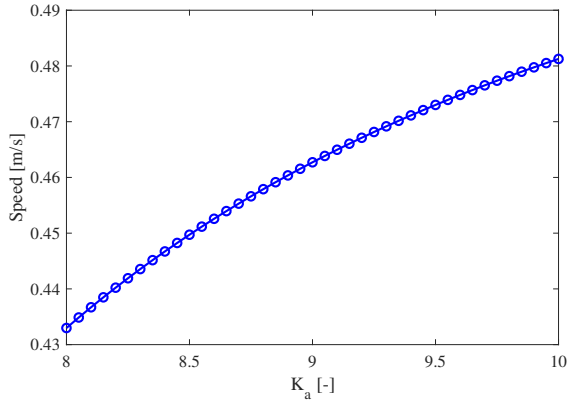

Fig. 17. Walking speed of RW-3 with respect to the amplitude of the wobbling mass

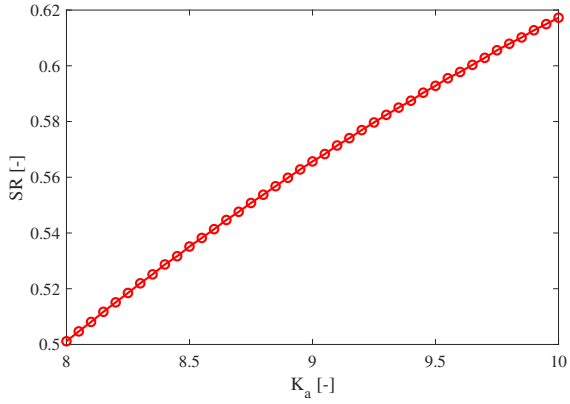

Fig. 18. SR of RW-3 with respect the amplitude of the wobbling mass

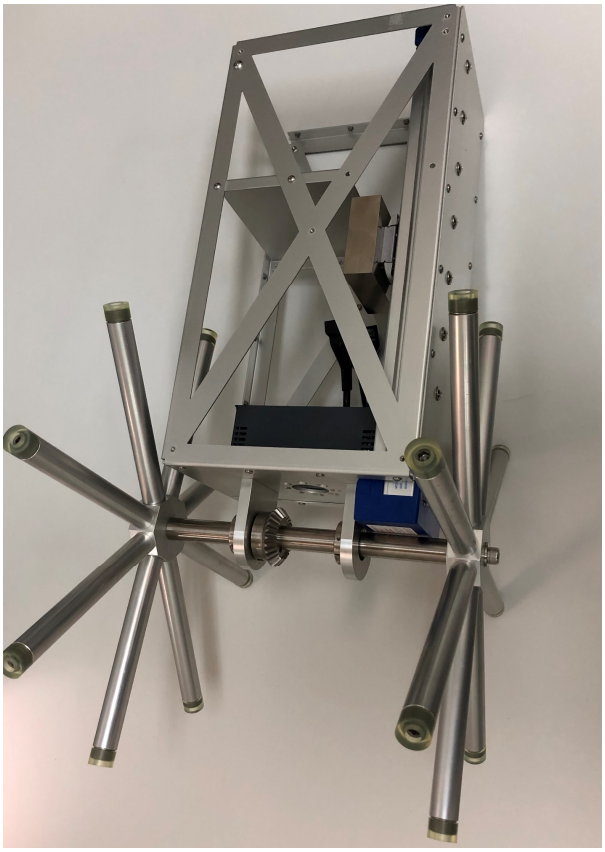

Fig. 19. Prototype of RW-3

[8] Y. Hanazawa, H. Suda, Y. Iemura, and M. Yamakita, "Active walking robot mimicking flat-footed passive dynamic walking," in *Proc. IEEE International Conference on Robotics and Biomimetics (ROBIO)*, 2012, pp. 1281–1286.

[9] Y. Hanazawa and F. Asano, "High-speed biped walking using swinging-arms based on principle of up-and-down wobbling mass," in *Proc. IEEE International Conference on Robotics and Automation (ICRA)*, 2015, pp. 5191–5196.

[10] J. Kawamoto and F. Asano, "Active viscoelastic-legged rimless wheel with upper body and its adaptability to irregular terrain," in *Proc. IEEE/RSJ International Conference on Intelligent Robots and Systems (IROS)*, 2012, pp. 157–162.

[11] F. Asano and J. Kawamoto, "Modeling and analysis of passive viscoelastic legged rimless wheel that generates measurable period of double-limb support," *Multibody System Dynamics*, vol. 31, no. 2, pp. 111–126, 2013.

[12] Y. Hanazawa, T. Hayashi, M. Yamakita, and F. Asano, "High-speed limit cycle walking for biped robots using active up-and-down motion control of wobbling mass," in *Proc. IEEE/RSJ International Conference on Intelligent Robots and Systems (IROS)*, 2013, pp. 3649–3654.

[13] J. W. Grizzle, G. Abba, and F. Plestan, "Asymptotically stable walking for biped robots: Analysis via systems with impulse effects," *IEEE Transactions on Automatic Control*, vol. 46, no. 1, pp. 51–64, 2001.